

## Supplementary Information

# Adeno-Associated Virus Characterization for Cargo Discrimination through Nanopore Responsiveness

Buddini Iroshika Karawdeniya<sup>1, \*</sup>, Y. M. Nuwan D. Y. Bandara<sup>1, \*</sup>, Aminul Islam Khan<sup>2, \*</sup>, Wei Tong Chen<sup>3</sup>, Hoang-Anh Vu<sup>4</sup>, Adnan Morshed<sup>2</sup>, Junghae Suh<sup>3, 4, 5, 6</sup>, Prashanta Dutta<sup>2</sup>, and, Min Jun Kim<sup>1, #</sup>

<sup>1</sup>Department of Mechanical Engineering, Southern Methodist University, Dallas, TX, 75275, USA

<sup>2</sup>School of Mechanical and Materials Engineering, Washington State University, Pullman, WA, 99164, USA

<sup>3</sup>Department of Chemical and Biomolecular Engineering, Rice University, Houston, TX, 77005, USA

<sup>4</sup>Department of Bioengineering, Rice University, Houston, TX, 77005, USA

<sup>5</sup>Department of Biosciences, Rice University, Houston, TX, 77005, USA

<sup>6</sup>Systems, Synthetic, and Physical Biology Program, Rice University, Houston, TX, 77005, USA

\* Authors contributed equally

#Corresponding author: mjkim@lyle.smu.edu

## Table of Contents

Section 1: Construction of $\Delta I/I_0$ histograms and Gaussian fitting .....	2
Section 2: Percentage difference in $\Delta I/I_0$ with respect to AAV with no encapsulated DNA .....	2
Section 3: TEM image and I-V curve of a nanopore and cell-schematic .....	3
Section 4: Data for Deep Neural Network Training and Validation .....	4
Section 5: Open-pore current variation with and without AAV .....	4
Section 6: Electro-deformation based flagging of AAV <sub>empty</sub> in a spiked sample. ....	6

## Section 1: Construction of $\Delta I/I_0$ histograms and Gaussian fitting

The histograms shown in Figure 2 were constructed using the in-built *Histogram* function of Mathematica 11.0.1.0 (Wolfram, USA) with a custom binwidth of 0.1. The histograms were then fitted with a single Gaussian in the form

$$A_i \exp\left(-\left(\frac{\Delta I}{I_0} - \mu_i\right)^2 / \sigma_i^2\right) \quad \text{Eq. S1}$$

where  $A_i$ ,  $\mu_i$ ,  $\sigma_i$  and  $\frac{\Delta I}{I_0}$  are amplitude, mean, standard deviation and relative current change (independent variable), respectively. For ease of representation,  $\Delta I/I_0$  is multiplied by 1000 (Figure 2). The fitting was done using *non-linear-model-fit* function of Mathematica in *automatic* mode.

## Section 2: Percentage difference in $\Delta I/I_0$ with respect to AAV with no encapsulated DNA

Percentage  $\Delta I/I_0$  difference is defined as,

$$\%(\Delta I/I_0)_{(empty,i)} = \frac{\left(\frac{\Delta I}{I_0} \times 1000\right)_i - \left(\frac{\Delta I}{I_0} \times 1000\right)_{empty}}{\left(\frac{\Delta I}{I_0} \times 1000\right)_{empty}} \times 100 \quad \text{Eq. S2}$$

where  $\left(\frac{\Delta I}{I_0} \times 1000\right)_i$  is the relative current drop of AAV encapsulating dsDNA or ssDNA at a given voltage multiplied by 1000.

### Section 3: TEM image and I-V curve of a nanopore and cell-schematic

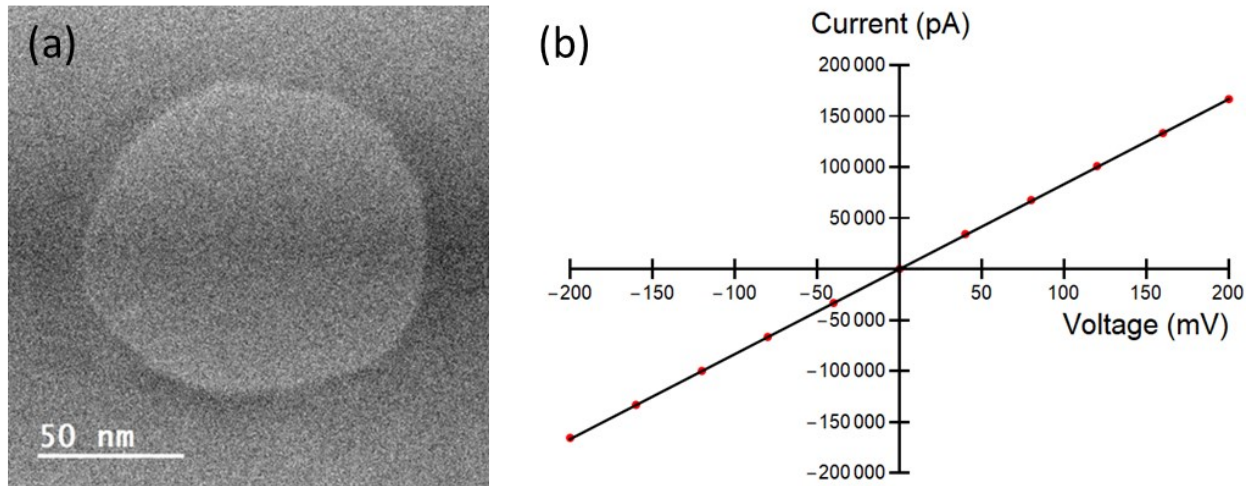
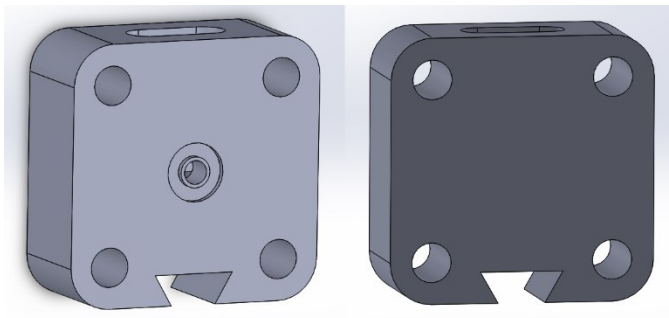


**Figure S1:** (a) A representative TEM image and an (b) I-V (current-voltage) curve of a nanopore  $\sim 100$  nm in diameter used for the experiments. 1 M KCl buffered at pH $\sim 7$  (phosphate buffer saline (P5493, Sigma-Aldrich, USA)) was used to obtain the I-V curve, and the diameter was estimated



using Equation 1.

**Figure S2:** 3D schematic of the custom flow-cell used for experiments

## Section 4: Data for Deep Neural Network Training and Validation

Voltage (mV)	AAVs	Number of Images (Training/Validation)			Mean Accuracy (Raw/Transformed) (%)			Overall Accuracy (Raw/Transformed) (%)		
		1 sec	2 sec	4 sec	1 sec	2 sec	4 sec	1 sec	2 sec	4 sec
175	Empty	816/204	408/102	204/51	77.6/88.7	83.9/95.2	79.4/95.7	81.6/94.0	83.5/95.4	87.9/96.9
	ssDNA	928/232	464/116	232/58	78.8/97.5	79.5/94.5	94.1/97.2			
	dsDNA	438/110	219/55	110/27	95.0/96.6	90.9/98.9	90.7/98.5			
150	Empty	480/120	240/60	120/30	82.6/94.5	82.8/94.3	92.7/96.4	83.1/95.2	90.9/96.2	92.4/96.2
	ssDNA	723/181	362/90	181/45	71.5/94.8	96.8/97.0	91.6/95.3			
	dsDNA	480/120	240/60	120/30	95.3/96.2	93.0/97.2	93/96.7			
100	Empty	493/123	246/62	123/31	82.0/86.7	83.4/89.5	79.7/87.7	85.6/88.4	87.2/90.5	86.7/92.3
	ssDNA	870/218	435/109	218/54	82.7/88.3	84.2/91.6	91.1/91.9			
	dsDNA	822/206	411/103	206/51	92.1/90.2	94.1/90.3	89.8/97.3			

**Table S1.** Summary of the AAVs dataset (number of images) and results (mean accuracy and overall accuracy). The different number of images are due to a different length of experiments for each class of virus. The accuracy of an individual class was obtained by dividing the number of correct predictions by the total number of test images for a particular category.

## Section 5: Open-pore current variation with and without AAV

During viral particle transit, the increase in resistivity is related to the lower electrical conductivity of the virus. Thus, we tested out different internal conductivities ( $\sigma_{in}$ ) over the physiologically relevant range and singled out specific values of  $\sigma_{in}$  for each of the different AAVs which matched the experimental current profile (Figure S3a-c). These (internal) conductivity values and the resulting conductivity ratio are presented in Table S2 for an external medium electrical conductivity of 12 S/m (corresponding to 2M LiCl). It is interesting to note the increase in

conductivity as the AAV cargo type changes from empty to single-stranded and double-stranded DNA. Both experimental and numerical results for the background current variation (inset, Figure S3a-c) reveal the underlying linear, Ohmic nature of the ionic currents. The Ohmic nature also means if the virus does not physically deform during translocation through the pore, the ratio of the current drop and the background current ( $\Delta I/I_0$ ) must remain unchanged. This is expected because both quantities in the ratio scale linearly at the same rate with increasing voltage when the electrical properties remain unchanged. However, the experimental data (Figure 2d) clearly deviate from this behavior and show a decrease in  $\Delta I/I_0$  consistently for all three AAV types as the applied voltage is increased. This behavior is an indication of the mechanical deformation of the virus when it travels through the pore.

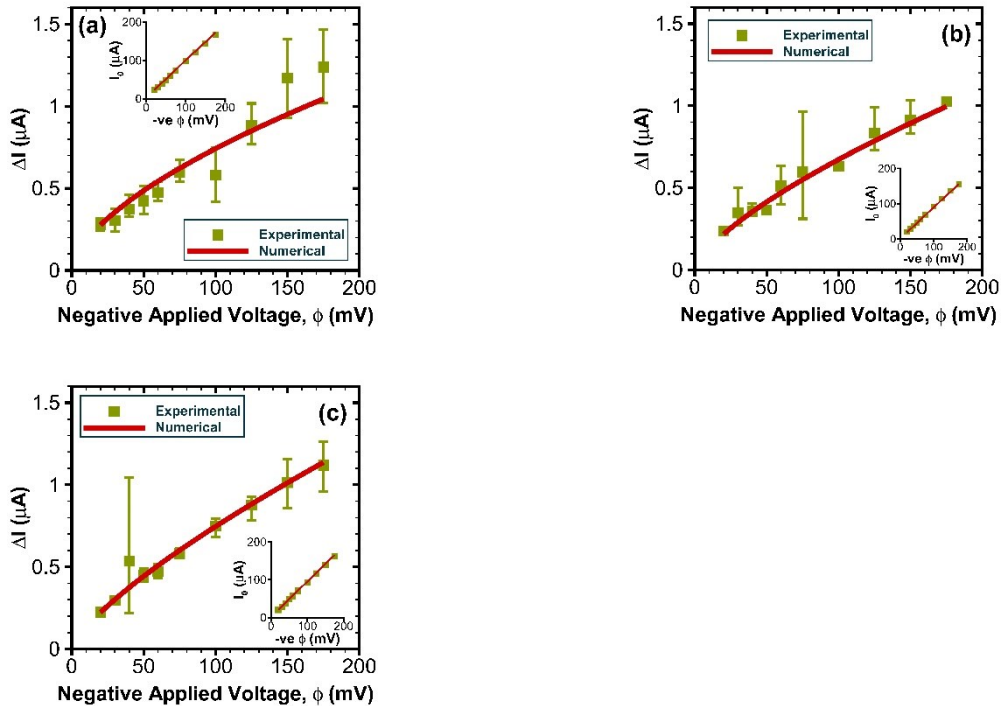


**Figure S3:** Current drop for (a)  $\text{AAV}_{\text{empty}}$ , (b)  $\text{AAV}_{\text{ss-DNA}}$ , and (c)  $\text{AAV}_{\text{ds-DNA}}$  samples for different negative applied voltages. The background currents (without any virus) for the same voltage range in all three cases are shown in inset. Arithmetic mean of three sets of independent experimental data (green

squares), as well as their upper and lower bounds, is presented along with the numerical predictions (solid red line).

<b>Virus Type</b>	<b>Inner Conductivity (S/m)</b>	<b>Conductivity Ratio, <math>\lambda</math></b>
<b>AAV<sub>empty</sub></b>	0.5	0.0417
<b>AAV<sub>ss-DNA</sub></b>	0.65	0.0542
<b>AAV<sub>ds-DNA</sub></b>	0.7	0.0583

**Table S2:** Predicted viral conductivity variation with different cargo content

### **Section 6: Electro-deformation based flagging of AAV<sub>empty</sub> in a spiked sample.**

For an AAV<sub>ds-DNA</sub> aliquot spiked with a significant amount of AAV<sub>empty</sub> (~75% AAV<sub>empty</sub> and ~25% AAV<sub>ds-DNA</sub>), we fitted each normalized current change (indicator of deformation) with a single Gaussian. A closer inspection of the histograms corresponding to normalized current profiles of the spiked sample (Figure 4b), it is clear, that the population cannot be well fitted with a single Gaussian. This deviation is apparent at lower voltages – a clear population outside the Gaussian fit exist at higher  $\Delta I/I_0$ . It is interesting to note, in Figure S4, the profile corresponding to the mixture has a higher deformation compared to the two individual components in the mixture. A mixture is in fact more complex than sample consisting of a single AAV type and this improbability could be due to presence of the two-populations (AAV<sub>empty</sub> and AAV<sub>ds-DNA</sub>) alienating the possibility of properly fitting the deformation profile with a single Gaussian.

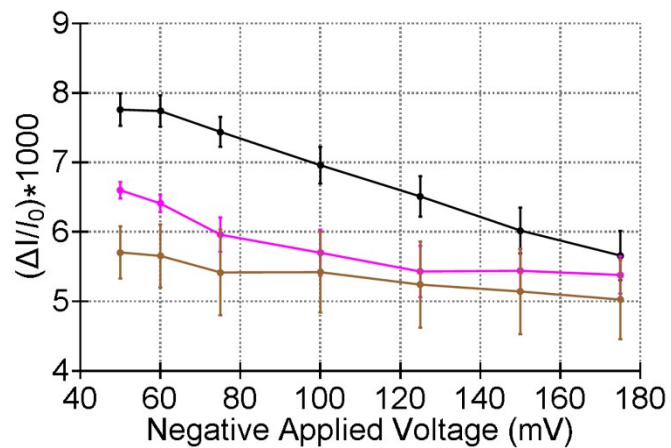


**Figure S4:** Deformation metrics ( $\Delta I/I_0$  versus voltage) corresponding to AAV<sub>ds-DNA</sub> (black; from 3 unique pores), AAV<sub>empty</sub> (magenta; from 3 unique pores) and a 75:25% (in concentration) of AAV<sub>Empty</sub> and AAV<sub>ds-DNA</sub> (brown; from 2 unique pores).